Vibrational Relaxation Dynamics of *trans*-Stilbene in the Lowest Excited Singlet State. Pump and Probe Wavelength Dependencies of the Picosecond Time-Resolved Anti-Stokes Raman Spectrum

Takakazu Nakabayashi,[†,‡] Hiromi Okamoto,[*,†] and Mitsuo Tasumi[§]

Department of Chemistry and Research Centre for Spectrochemistry, School of Science, The University of Tokyo, Bunkyo-ku, Tokyo 113-0033, Japan, and Department of Chemistry, Faculty of Science, Saitama University, Urawa, Saitama 338-8570, Japan

Received: May 19, 1998; In Final Form: September 22, 1998

The vibrational relaxation process of *trans*-stilbene in the lowest electronically excited singlet state after photoexcitation has been studied by picosecond time-resolved anti-Stokes Raman spectroscopy using several pump and probe wavelengths. Measurements of pump wavelength dependency have shown that, when the molecules are excited by pump photons with a high excess vibrational energy (∼5200 cm^{-1}), part of the excess vibrational energy remains localized in the olefinic C═C stretching (ν_7) and the C−Ph stretching (ν_{15}) modes for a period within the time resolution of the present measurements (∼5 ps) after photoexcitation. Analysis of the probe wavelength dependency has indicated that the vibrationally excited transients observed in the picosecond anti-Stokes Raman spectra are for the most part in the lowest excited vibrational levels ($n = 1$), as far as the ν_7 and ν_{15} modes are concerned. From these results it is suggested that the intramolecular vibrational relaxation process proceeds in roughly two steps. The optically pumped molecules on highly excited vibrational levels of the olefinic stretching modes first relax very rapidly (probably in the femto to subpicosecond time range) to the lowest vibrationally excited state. Then, slower relaxation occurs in several picoseconds to achieve an intramolecular (quasi) thermal equilibrium.

1. Introduction

The study of chemical reactions in the condensed phase aims at characterizing reaction coordinates and interactions among reactants and solvents, for the ultimate purpose of finding, if possible, ways to control the chemical reactions. Vibrational population relaxation process (simply called in this paper "vibrational relaxation"), which is defined as the transition process from a vibrationally excited state to a thermodynamically favorable state, plays key roles in ultrafast chemical reactions. In photophysics and photochemistry, vibrational relaxation is regarded as one of the earliest molecular processes, immediately after photoexcitation. Vibrational relaxation processes compete with ultrafast geometric changes (reactions) such as photoisomerization, photodissociation, etc. and have significant effects on the rates, pathways, and efficiencies of these processes. Detailed knowledge of vibrational relaxation is therefore essential for elucidating the mechanisms of ultrafast reactions. A number of experimental and theoretical studies have been devoted to understanding the mechanisms of vibrational relaxation and have been reviewed from various perspectives.[1−7]

In solution, vibrational relaxation is considered to proceed in several steps.[5] Immediately after photoexcitation and/or nonradiative electronic transition, excess vibrational energy [difference between energies of the pump photon and the origin of the absorption spectrum (i.e., 0−0 transition)] is localized on Franck−Condon active vibrational modes. The localized excess energy is first distributed to other vibrational modes within the solute molecule [intramolecular vibrational redistribution (IVR)]. The IVR process is completed with very rapid randomization of the excess energy and creates a quasiequilibrium among all the intramolecular vibrational modes of the solute molecule,[8] resulting in a single, mode-independent vibrational temperature. At this stage, the temperature is higher than that of the surrounding molecules. The vibrationally hot molecule then dissipates its excess energy to the surrounding solvent molecules through intermolecular interactions [vibrational cooling (VC)].

The kinetics of vibrational relaxation depends strongly on the molecule under study.[6] For medium-sized to large molecules in solution, an empirical rule that the typical time scale of IVR is in the subpicosecond range and that of VC in tens of picoseconds has been proposed from a number of data on vibrational relaxation.[5] Until recently, it has been believed that this rule is widely applicable to systems in the liquid phase. However, several recent experimental results suggest that the IVR process occurs in the time range of several picoseconds, even for large molecules in solution.[9−23] Whether or not the excess vibrational energy is statistically distributed very rapidly among intramolecular vibrational modes is an important question that is closely related to reaction dynamics. There is fundamental importance, therefore, in investigating the IVR process in more detail to understand the mechanisms of photochemical processes and to obtain guidelines for the control of reactions in solution.

Much of the recent development in studies of vibrational relaxation dynamics is due to the progress in ultrafast laser spectroscopy, which enables a direct time-domain observation

* To whom correspondence should be addressed. E-mail: aho@music.email.ne.jp.
† The University of Tokyo.
‡ Present address: Institute for Molecular Science, Myodaiji, Okazaki, Aichi 444-8585, Japan.
§ Saitama University.

10.1021/jp982287g CCC: $15.00
Published on Web 10/30/1998

of changes in populations on vibrational levels. Among various methods, time-resolved anti-Stokes Raman spectroscopy is one of the powerful tools for studying vibrational relaxation dynamics in solution. This method is based on the pump and probe sequence, where a (strong) pump pulse creates a nonequilibrium population distribution on vibrational levels and the anti-Stokes resonance Raman spectrum arising from the vibrationally excited species is monitored by a (weak) probe pulse coming after the pump pulse. It probes only those molecules that are populated in excited vibrational states and hence provides state-specific dynamic information that is essential for a detailed understanding of vibrational relaxation. Several groups have recently reported transient anti-Stokes Raman spectra of vibrationally hot molecules to obtain information on the IVR and VC processes in solution.[14−33] We have recently demonstrated that anti-Stokes resonance Raman excitation profiles (REPs), that is, plots of the probe wavelength dependencies of anti-Stokes resonance Raman intensities, are useful for determining the energy levels of vibrationally excited molecules observed in time-resolved anti-Stokes Raman spectra.[23,32,33]

In the present paper, we report picosecond anti-Stokes Raman studies on the vibrational relaxation dynamics of *trans*-stilbene in the lowest excited singlet (S_1) state in solution, paying special attention to the pump and probe wavelength dependencies. A preliminary account of this study has been published.[23] Details of the experimental results and more advanced analyses are described in the present paper. Time-resolved Stokes Raman spectroscopy has made a noticeable contribution in revealing the character of *trans*-stilbene in the S_1 state in solution.[34,35] Assignments of the Raman bands of *trans*-stilbene in the S_1 state have been examined to such an extent that they can be used to gain some insight into the structural changes occurring on photoexcitation from observed spectra.[34,35] Several groups have recently reported the anti-Stokes Raman spectra of *trans*-stilbene in the S_1 state in the wavenumber region of 1600−200 cm^{-1}.[18−20,23] From an analysis of temporal behavior of the anti-Stokes Raman intensities, Jean and co-workers[18,19] have suggested that a nonstatistical distribution of excess energy among intramolecular vibrational modes persists for several picoseconds after photoexcitation. This means that it takes at least several picoseconds to complete the IVR process. This result is regarded as an example of the relatively slow IVR mentioned earlier, and further experimental studies are essential to understand vibrational relaxation in more detail.

The contents discussed in this paper are as follows. We first examine the pump and probe laser power dependencies of the anti-Stokes Raman spectra of *trans*-stilbene in the S_1 state to confirm the absence of nonlinear responses, which make subsequent analyses difficult. Next, we analyze the pump wavelength dependency of the anti-Stokes Raman spectra to obtain information on the distribution of excess vibrational energy among intramolecular modes. Third, we simulate the observed probe wavelength dependency of the anti-Stokes spectra to determine the energy levels on which the observed vibrationally excited transients are populated. Finally, the vibrational relaxation process of *trans*-stilbene in the S_1 state in solution is discussed on the basis of the results obtained.

2. Experimental Section

The spectrometer used for the time-resolved Raman measurements was basically the same as that described previously.[33] Briefly, a beam from a frequency-doubled CW mode-locked Nd:YLF laser (Quantronix 4216D; wavelength, 527 nm; repetition rate, 82 MHz; average power, 2 W; pulse duration, 60 ps) was used to excite two synchronously pumped dye lasers (Spectra-Physics/Quantronix 3500). Light pulses with ∼3 ps duration and ∼1 nJ pulse energy were obtained. Pulses from the dye lasers passed through dye amplifiers (Leonix), and amplified pulses with pulse energies of 5−50 μJ were obtained at a repetition rate of 1 kHz. The dye amplifiers were excited by the second harmonic of the output from a CW Nd:YLF regenerative amplifier (Quantronix 4417RG, 527 nm, 1 kHz, 1.2 W, 60 ps) seeded by the CW mode-locked Nd:YLF laser.

Since ultraviolet radiation is needed to excite the $S_1 \leftarrow S_0$ transition of *trans*-stilbene, the output from one of the dye amplifiers was frequency-doubled to obtain the pump beam. The output from the other amplified dye laser was used as the probe beam for resonance Raman observation. The probe wavelength was tuned in the region between 550 and 670 nm. To reduce disturbance caused by unamplified dye laser pulses at 82 MHz in the Raman spectra, an acousto-optic modulator (HOYA A-140−633) was placed before the dye amplifier.

After passing through fixed (for the pump beam) and variable (for the probe beam) optical delay lines, the pump and probe beams, which were polarized in the same direction, were superimposed by a dichroic mirror and focused onto the sample solution with an $f = 70$ mm lens. The focused area was $\sim 1 \times 10^{-3}$ cm^2. The sample solution flowed through a squeezed stainless steel nozzle to form a thin (∼0.3 mm) liquid jet. For Raman measurements in the low-wavenumber region (<300 cm^{-1}), a narrow band-pass filter (CVI, full-width at half-maximum ≈ 10 nm) was used to eliminate the background emission from the dye amplifier, which seriously interfered with Raman observation in the low-wavenumber region. Because of the timing jitter between the pump and probe pulses, the temporal resolution of the system (5−7 ps) was lower than the pulse duration of a few picoseconds.[36]

For measurements of delay time dependencies and those of incident laser power dependencies, an experimental configuration with only one amplified dye laser was also adopted. In this configuration, the second harmonic output of the dye amplifier was used as the pump beam and the visible radiation, which remained unconverted, was used as the probe beam. Time resolution in this case was determined by the autocorrelation width of the pulses from the dye laser (3−4 ps).

The 90°-scattered Raman signal was collected and dispersed by a triple polychromator and detected by a CCD detector. The spectral slit width was ∼10 cm^{-1}. The typical exposure time was 10 min for the Stokes Raman measurements and 60 min for the anti-Stokes Raman measurements. *trans*-Stilbene of special reagent grade was purchased from Tokyo Kasei Co. and used without further purification. 1-Butanol (solvent) of liquid chromatography grade from Wako Pure Chemicals Co. was used as received. The concentration of the sample solution was $(1-5) \times 10^{-3}$ mol dm^{-3}. All experiments were carried out at room temperature.

3. Results

The discussion in this paper is based upon the assignments of the Raman bands of *trans*-stilbene in the S_1 state[34,37] and the vibrational-mode numbering given by Urano et al.[37] The vibrational bands of *trans*-stilbene in the S_1 state observed in the transient Raman spectra (Figures 1, 2, and 4−6) may be roughly classified into two groups, one consisting of bands due to the olefinic vibrations and the other including bands due to the phenyl ring vibrations. The three most prominent Raman bands are ascribed to the olefinic vibrations. The relatively broad Raman band at ∼1570 cm^{-1} (ν_7) is assigned to the olefinic

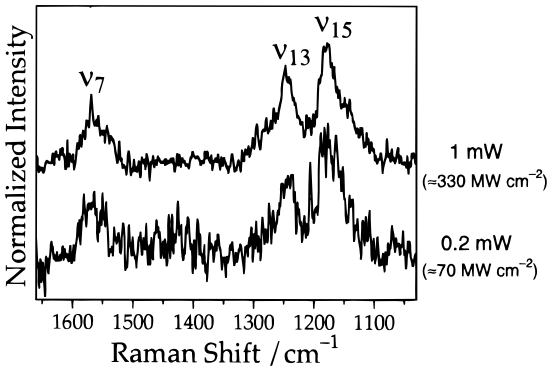

Figure 1. Pump laser power dependency of the anti-Stokes Raman spectra of *trans*-stilbene in the S_1 state at 0 ps delay time. The intensity of each spectrum is normalized by the pump laser power. The average pump laser power and the approximate value of peak power density of the pump pulse (in parentheses) are given on the right side of each spectrum. Pump, 277 nm; probe, 610 nm.

C═C stretch, and the band at ∼1240 cm^{-1} (ν_{13}) is attributed to the olefinic C−H in-plane bend. Another band at ∼1180 cm^{-1} (ν_{15}) is due to a mode with a major contribution from the C−Ph stretch.[34,37] On the other hand, the two peaks at ∼1530 (ν_8) and ∼1147 cm^{-1} (ν_{16}) are assigned to the phenyl C═C stretch and the phenyl C−H bend, respectively.

3.1. Incident Laser Power Dependencies of Anti-Stokes Raman Spectra. In ultrafast time-resolved Raman spectroscopy, very strong radiation of the incident laser pulses often induces unfavorable nonlinear effects, which make analyses difficult. Iwata and Hamaguchi have reported that peak positions and bandwidths of the transient Stokes Raman bands change when the peak powers of incident laser pulses are very high.[38] We first examine the pump and probe laser power dependencies of the anti-Stokes Raman spectra of *trans*-stilbene in the S_1 state.

The anti-Stokes Raman spectra of *trans*-stilbene in the S_1 state at 0 ps delay time observed with two different magnitudes of the pump laser power are shown in Figure 1, where the observed three bands are attributed to the S_1 state. The intensity of each spectrum is normalized by the pump laser power. When the pump photon density is very high, the S_1 species (generated by the $S_1 \leftarrow S_0$ optical transition) may absorb another pump photon to generate a higher electronically excited (S_m) state. If a very rapid internal conversion from S_m to S_1 occurs, vibrationally excited transients in the S_1 state may be generated and observed in the anti-Stokes Raman spectra. In this case, anti-Stokes Raman intensities should show a quadratic dependency on the pump laser power. From comparison of the normalized intensities of corresponding bands in Figure 1, it is found that the normalized anti-Stokes intensities are independent of the pump laser power. This means that the anti-Stokes intensities are linearly proportional, within the experimental accuracy, to the pump laser power at least up to 1 mW. The band shapes and peak positions of the anti-Stokes Raman bands and their relative intensities are independent of the pump-laser power. This result indicates that the two- (or multi-) photon process of the ultraviolet pump radiation has only negligible effects, if any, on the anti-Stokes Raman spectra of *trans*-stilbene in the S_1 state.

The probe laser power dependency should also be examined. When the probe photon density is very high, the S_1 species may be further excited to a higher electronically excited (S_n) state by absorbing the visible probe photon. The $S_n \rightarrow S_1$ internal conversion process may populate vibrationally excited states of the S_1 species, which would give rise to the anti-Stokes

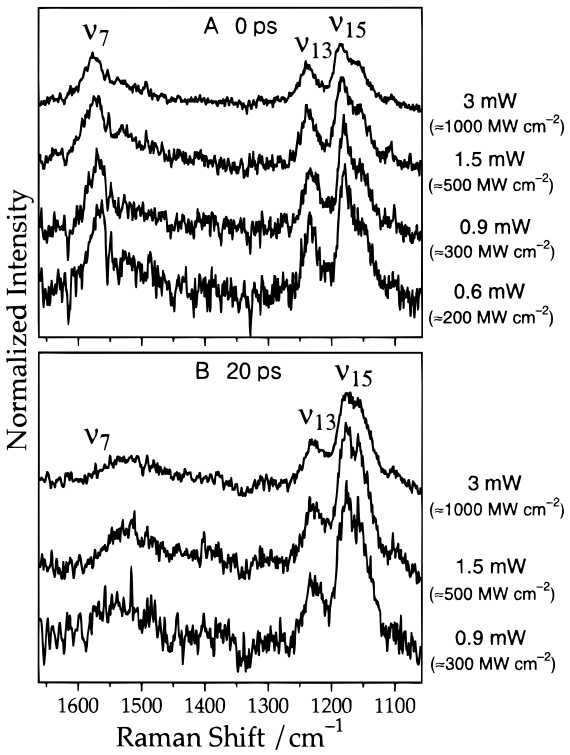

Figure 2. Probe laser power dependency of the anti-Stokes Raman spectra of *trans*-stilbene in the S_1 state at 0 ps (A) and 20 ps (B) delay times. The intensity of each spectrum is normalized by the probe laser power. The average probe laser power and the approximate value of peak power density of the pump pulse (in parentheses) are given on the right side of each spectrum. Pump, 303 nm; probe, 606 nm (the pump beam was the second harmonic of the probe beam).

Raman scattering. In this case, the anti-Stokes Raman spectral pattern should not be strongly dependent on the delay time between the pump and probe pulses in the range shorter than ∼20 ps, in view of the slow $S_1 \rightarrow S_0$ internal conversion (∼60 ps). In addition, the anti-Stokes intensities should exhibit a quadratic dependency on the probe laser power. Panels A and B in Figure 2 show the probe laser power dependencies of the anti-Stokes Raman spectra of *trans*-stilbene in the S_1 state at 0 and 20 ps delay times, respectively. The intensity of each spectrum is normalized by the probe laser power. If we compare the spectra shown in Figure 2A and Figure 2B, clear differences in the delay time dependency are observed among bands attributed to the S_1 species. When the probe laser power is low (less than ∼1 mW in Figure 2A and less than ∼1.5 mW in Figure 2B), the anti-Stokes Raman intensities are approximately proportional to the probe laser power. As the probe laser power is increased beyond these values, the Raman intensities seem to saturate. The signals begin to show sublinear dependencies on the probe laser power. The sublinear dependency on the probe laser power may be partly due to the depletion of the S_1 species by the $S_n \leftarrow S_1$ photoexcitation. Even in this power range, the relative intensities among the Raman bands are independent of the probe laser power. In any power range, a quadratic (or higher-order) dependency of the anti-Stokes Raman intensities on the probe laser power is not observed. This result indicates that higher order nonlinear effects of the probe photons are negligible in the anti-Stokes Raman spectra of *trans*-stilbene in the S_1 state.

From the results described above, it is concluded that the observed anti-Stokes Raman bands arise from vibrationally excited transients in the S_1 state generated from the S_0 state by absorbing *one* pump photon.

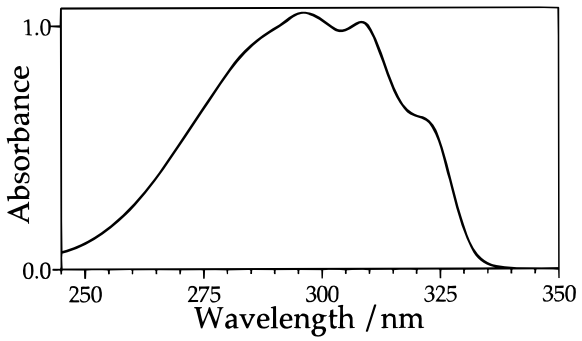

Figure 3. Electronic absorption spectrum of *trans*-stilbene in a 1-butanol solution at room temperature; sample concentration $\approx 4 \times 10^{-4}$ mol dm^{-3}.

3.2. Pump Wavelength Dependency of Anti-Stokes Raman Spectra. Figure 3 shows the $S_1 \leftarrow S_0$ absorption spectrum of *trans*-stilbene in a 1-butanol solution. The second derivative of the absorption spectrum shows that the 0−0 transition of the $S_1 \leftarrow S_0$ absorption is located at ~30 880 cm^{-1} (323.8 nm). It is known that the vibronic structure of the $S_1 \leftarrow S_0$ absorption spectrum arises mainly from the olefinic stretching modes (C=C and C−Ph stretches).[37,39,40] Two different pump wavelengths used in the transient Raman measurements are 277 nm (hereafter called the short-wavelength pump or briefly SWP) and 320 nm (the long-wavelength pump or LWP). The SWP light corresponds to an energy ~5200 cm^{-1} above the 0−0 transition of the $S_1 \leftarrow S_0$ absorption. Such an amount of excess vibrational energy may produce substantial populations on highly excited vibrational levels of the Franck−Condon active olefinic vibrational modes immediately after photoexcitation. On the other hand, the LWP light corresponds to an energy only ~400 cm^{-1} above the 0−0 transition. With the LWP, high-wavenumber modes cannot be excited on the $S_1 \leftarrow S_0$ photoexcitation. If high-wavenumber anti-Stokes Raman bands are observed, it should be attributed to thermally populated molecules at room temperature.

In Figure 4, the anti-Stokes Raman spectra of *trans*-stilbene in the S_1 state at 0 and 20 ps delay times are shown. Each spectrum is normalized to the intensity of the ν_{15} band. The upper two traces are the SWP spectra (excess vibrational energy $\approx$ 5200 cm^{-1}). The absolute band intensities are found to decay with a time constant of ~10 ps (depending to some extent on the observed bands). Generally speaking, anti-Stokes Raman intensities are weak in the high-wavenumber region because of smaller vibrationally excited populations. This general rule does not hold, however, in the SWP spectrum at 0 ps delay time. The anti-Stokes Raman intensity of the ν_7 band (1570 cm^{-1}) is comparable to those of the ν_{13} and ν_{15} bands (around 1200 cm^{-1}). The intensities of the bands in the SWP spectra show different delay time dependencies. For example, the intensity of the ν_7 band decreases much faster than those of the ν_{13} and ν_{15} bands.

The lower two traces are the LWP spectra (excess vibrational energy $\approx$ 400 cm^{-1}). In contrast to the SWP spectra, the relative intensities of the bands are independent of the delay time. The absolute band intensities are also found to remain almost unchanged up to 20 ps. The features of the LWP spectra are very similar to those of the SWP spectrum at 20 ps delay time.

3.3. Probe Wavelength Dependency of Stokes and Anti-Stokes Raman Spectra. Figure 5 shows the Stokes Raman spectra of *trans*-stilbene in the S_1 state at 30 ps delay time observed with several probe wavelengths in resonance with the $S_n \leftarrow S_1$ absorption. Since the VC process in *trans*-stilbene in the S_1 state is considered to occur in tens of picoseconds,[35,41] molecules giving rise to the Stokes Raman scattering at 30 ps delay time would be mostly on the ground vibrational ($n = 0$) level.

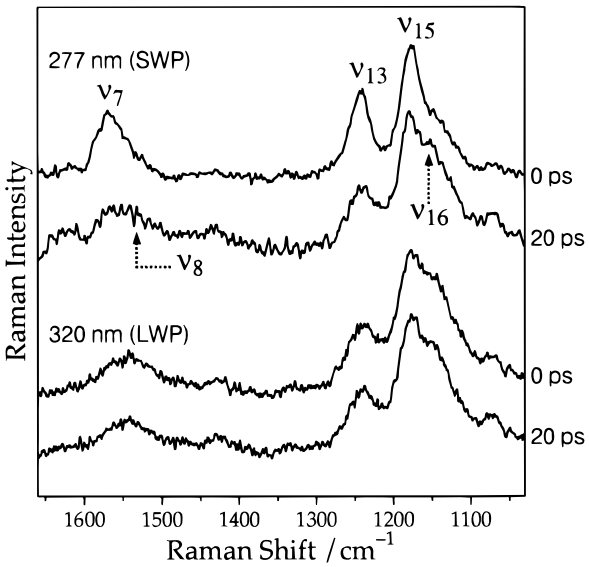

Figure 4. Pump wavelength dependency of the anti-Stokes Raman spectra of *trans*-stilbene in the S_1 state. The intensity of each spectrum is roughly normalized by reference to the intensity of the ν_{15} band at 1180 cm^{-1}. Pump wavelength, 277 nm (SWP) for the upper two spectra and 320 nm (LWP) for the lower two spectra; probe wavelength, 610 nm. The delay time is given on the right side of each spectrum.

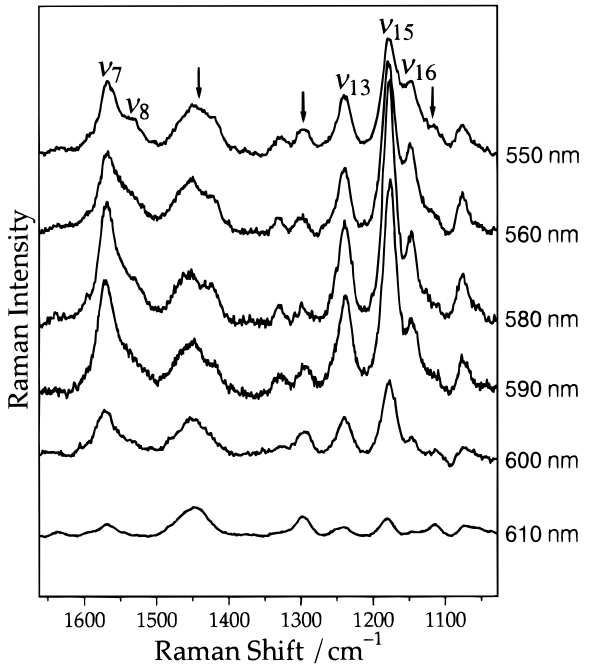

Figure 5. Probe wavelength dependency of the Stokes Raman spectra of *trans*-stilbene in the S_1 state at 30 ps delay time. Pump, 277 nm; probe, given on the right side of each spectrum. The intensity of each spectrum is roughly normalized by reference to the intensities of Raman bands of 1-butanol (indicated with arrows; the Raman band of 1-butanol at 1450 cm^{-1} is overlapped with that of *trans*-stilbene in the S_1 state).

In Figure 5, the three strong Raman bands (ν_7, ν_{13}, and ν_{15}) gain their intensities when the probe wavelength approaches the $S_n \leftarrow S_1$ absorption maximum around 585 nm.[41] This means that these bands are resonantly enhanced in resonance with the $S_n \leftarrow S_1$ electronic transition. Each Raman band shows a characteristic probe wavelength dependency. For example, the

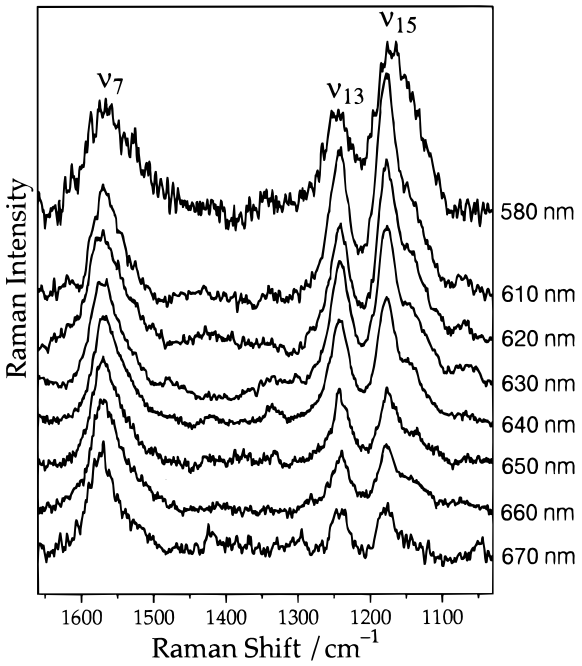

Figure 6. Probe wavelength dependency of the anti-Stokes Raman spectra of *trans*-stilbene in the S_1 state at 0 ps delay time. Pump, 277 nm; probe, given on the right side of each spectrum. The intensity of each spectrum is roughly normalized by reference to the intensity of the ν_7 band at 1570 cm^{-1}.

intensity of the ν_{15} band relative to that of the ν_7 band becomes higher if the probe wavelength is tuned around the maximum of the $S_n \leftarrow S_1$ absorption (585 nm).

The probe wavelength dependency of the anti-Stokes Raman spectra of *trans*-stilbene in the S_1 state at 0 ps is shown in Figure 6, where eight probe lights with wavelengths between 580 and 670 nm in resonance or preresonance with the $S_n \leftarrow S_1$ absorption are used. The three strong features (ν_7, ν_{13}, and ν_{15}) are observed in all the spectra shown in the figure. It has not been successful to obtain a good quality anti-Stokes Raman spectrum with the 580-nm probe light. Fluorescence arising from the $S_1 \rightarrow S_0$ transition seriously interferes with the Raman measurements in observing the wavelength region shorter than 545 nm. In addition, the anti-Stokes Raman intensities themselves are weak when the probe wavelength is set at 580 nm. These factors make it more difficult to observe the anti-Stokes spectrum with the 580-nm probe light. The intensity of the ν_{15} band relative to that of the ν_7 band shows a maximum at a 610 nm probe wavelength and decreases markedly with increasing probe wavelength. The relative intensity changes with the probe wavelength are much more prominent than those in the Stokes side.

Such a feature reflects the character of the observed vibrationally excited states. In the following discussion, the probe wavelength dependencies are quantitatively analyzed with a theoretical model to obtain information on vibrational relaxation dynamics. In the Raman intensity analyses, the best method is to evaluate the relative resonance Raman intensities by using a solvent Raman band as an internal intensity reference and to compare them with the simulated excitation profiles. However, this method is difficult in the present study for the following reasons. First, the solvent Raman bands are far weaker than the solute bands in the anti-Stokes spectra. Second, the concentration of the photoexcited transient is affected by fluctuation of the pump-pulse energy. In such a case, the Raman intensity relative to that of a solvent band has only a semiquantitative meaning. Instead, in the following analyses, we use the relative resonance Raman intensities of two bands, both of which are attributed to the S_1 species. Since the relative intensities of two Raman bands due to the same species are not affected by changes in the pump and probe laser power, their probe wavelength dependencies can be quantitatively analyzed.

4. Discussion

4.1. Pump Wavelength Dependency of Anti-Stokes Raman Spectra. In the SWP spectra in Figure 4, the intensity of the ν_7 band is comparable to those of the ν_{13} and ν_{15} bands at 0 ps delay time. In contrast, the relative intensity of the ν_7 band is much weaker in the 20 ps spectrum. This temporal behavior may be explained in terms of mode-dependent vibrational relaxation toward a thermal equilibrium. At 0 ps after photoexcitation under the SWP condition, the molecules in the S_1 state must have a large excess vibrational energy; the vibrationally excited populations must be greatly different from those under the thermal equilibrium at room temperature. The SWP spectrum at 0 ps delay time may be attributed to such molecules. It is considered that, at 20 ps delay time, most of the excess vibrational energy has dissipated to the solvent molecules and the vibrationally excited populations have reached the thermal equilibrium at room temperature. Accordingly, the 20-ps spectrum may be due to the molecules thermally populated on vibrationally excited levels. Then, the LWP spectra should give the spectral intensity pattern similar to that of the SWP spectrum at 20 ps and should show no delay time dependency, because the excess vibrational energy from the pumping photon is very small. The experimental results shown in the LWP spectra in Figure 4 agree well with this expectation. It can be hence concluded that the SWP spectrum at 0 ps arises from the vibrationally excited transients generated by the sufficient excess vibrational energy from the pumping photon.

The other two Raman bands indicated as ν_8 and ν_{16} in Figure 4 should also be noted. At 0 ps delay time, the intensity of the ν_{15} band relative to that of the ν_{16} band in the SWP spectrum is about twice as large as that in the LWP spectrum. A similar relation is found for the ν_7 and ν_8 bands. That is, the ν_{15} (or ν_7) band, which is located $\sim$30 cm^{-1} higher than the ν_{16} (or ν_8) band, is stronger in the SWP spectrum at 0 ps delay time than in the LWP spectrum. Then, we should first examine the possibility that this pump wavelength dependency is explained in terms of a difference in intramolecular vibrational temperature between the two spectra.

For that purpose, we need the transient intramolecular vibrational temperature immediately after the absorption of the pump photon. We estimate this temperature assuming a statistical distribution of the excess vibrational energy among all the intramolecular vibrational modes. Since it is hard to know precisely all the vibrational wavenumbers of *trans*-stilbene in the S_1 state in solution, we introduce an approximation that the vibrational modes of *trans*-stilbene (72 in total) lie at equal intervals between 0 and 1600 cm^{-1}, except for the C−H stretches (12 modes), which are assumed to have a single wavenumber of 3000 cm^{-1}. The temperature of the SWP-excited species (excess energy $\approx$ 5200 cm^{-1}) thus calculated is $\sim$550 K. This value should be regarded as a maximum value because the VC process is neglected. Since we have introduced a crude approximation for the vibrational wavenumbers, the calculated temperature may have an error of about $\pm$30 K, estimated from several trials on different vibrational wavenumber sets. As for the LWP-excited species, the intramolecular vibrational temperature can be assumed to be $\sim$300 K because of the very low excess energy.

Now we can calculate the populations on the lowest excited vibrational levels ($n = 1$) of the ν_{15} and ν_{16} modes on the basis of the Boltzmann distribution. The population on the $n = 1$ level of the ν_{15} mode at 550 K is estimated to be about 13 times as large as that at 300 K, while that for the ν_{16} mode at 550 K is about 12 times as large as that at 300 K. Consequently, the relative intensity of the two bands (ν_{15}/ν_{16}) in the SWP spectrum should be only ~1.1 (=13/12) times larger than that in the LWP spectrum. Obviously, this estimate does not agree with the corresponding observed value (~2). To explain the observed pump wavelength dependency on the basis of the Boltzmann distribution, the intramolecular vibrational temperature must be assumed to have an unrealistic value (much higher than 1000 K), which is clearly outside the uncertainty range of the calculated temperature. This is quite reasonable, because the energy difference between these two modes is only ~30 cm^{-1}. It is therefore concluded that the pump wavelength dependencies of the ν_{15} and ν_{16} Raman band intensities cannot be explained on the assumption of the statistical distribution of the excess vibrational energy among all the intramolecular vibrational modes. The excess energy is considered to be localized on the ν_{15} mode rather than on the ν_{16} mode in the photoexcited species observed in the SWP spectrum at 0 ps. A similar discussion can also be applied to the ν_7 and ν_8 vibrational bands; the excess vibrational energy is localized on the ν_7 mode rather than on the ν_8 mode in the SWP excited species at 0 ps delay time.

As mentioned earlier, the ν_7 and ν_{15} modes are attributed to the modes involving the olefinic stretching and are Franck−Condon active in the $S_1 \leftarrow S_0$ optical transition, while the ν_8 and ν_{16} modes are attributed to the phenyl ring vibrations. Consequently, the present results indicate that the SWP spectrum at 0 ps delay time arises from the vibrationally excited transients with the excess energy localized on the olefinic vibrational modes. Since the temporal resolution of the present experiment is 5−7 ps, it is concluded that it takes at least several picoseconds for *trans*-stilbene in the S_1 state to reach an intramolecular thermal equilibrium. In other words, the IVR process in *trans*-stilbene in the S_1 state is not complete within a few picoseconds.

4.2. Probe Wavelength Dependency of Stokes Raman Spectra. As mentioned earlier, photoexcitation of *trans*-stilbene by pumping photons with a high excess energy may populate highly excited vibrational levels of the Franck−Condon active olefinic modes. In subsection 4.1, it has been shown that the SWP anti-Stokes Raman spectrum at 0 ps arises from molecules before they reach an intramolecular thermal equilibrium. Then, the anti-Stokes Raman bands in the SWP spectrum at 0 ps may be due to molecules of either one of the following two cases: transients vibrationally highly excited (vibrational quantum number $n > 1$) in the olefinic vibrational modes or those not highly excited ($n \approx 1$) but with part of the excess energy still localized on the olefinic modes. It is important to clarify the vibrational levels on which such excited transients are populated for studying the mechanisms of vibrational relaxation dynamics. In the previous studies,[23,32,33] the present authors have demonstrated that anti-Stokes REP is useful for determining the energy levels on which vibrationally excited transients are populated. A preliminary report on the application of this method to *trans*-stilbene in the S_1 state has been already published.[23] In this paper, details of the analysis including a more advanced treatment on the contribution of a low-frequency vibrational mode are described.

To analyze the probe wavelength dependency of anti-Stokes Raman intensities, several parameters necessary for the calculation of anti-Stokes REPs must be determined first by analyzing the Stokes REPs and the $S_n \leftarrow S_1$ absorption spectrum. The theoretical model used for the calculation of the Stokes REPs and the $S_n \leftarrow S_1$ absorption is the same as that adopted for the case of a carotenoid.[32] It is based on the *A* term of Albrecht's formula (Franck−Condon mechanism). Only the *zz* component of the Raman tensor (a_{zz}) is taken into account, because the other components of the Raman tensor are considered to have negligible contributions to the intensities of the strong Raman bands of *trans*-stilbene in the S_1 state under a rigorous resonance condition.[42] The vibronic band shape of the absorption spectrum is assumed to be expressed by a simple convolution of the homogeneous (Lorentzian) and inhomogeneous (Gaussian) broadening functions.

The *zz* component of homogeneously broadened Raman tensor, $a_{zz}(\nu_0)$, for the f ← i transition from the initial (i) state to the final (f) state with the excitation frequency ν_0 is expressed as

$$a_{zz}(\nu_0) \propto \sum_{\mathrm{v}} \frac{\langle \mathrm{f}|\mathrm{v}\rangle\langle \mathrm{v}|\mathrm{i}\rangle}{E_{\mathrm{ev}} - E_{\mathrm{gi}} - h\nu_0 + \mathrm{i}\Gamma_{\mathrm{H}}} \tag{1}$$

where v represents a virtual state, E_{ev} and E_{gi} are the eigenenergies of the virtual and initial states, respectively, and Γ_{H} is the homogeneous bandwidth. The Raman intensity in photon numbers (not in radiation energy), $I_{\mathrm{f}\leftarrow\mathrm{i}}(\nu_0)$, including the inhomogeneous broadening, is then given as

$$I_{\mathrm{f}\leftarrow\mathrm{i}}(\nu_0) \propto \nu_{\mathrm{s}}{}^3 G(\nu')^* |a_{zz}(\nu_0)|^2 \tag{2}$$

$$G(\nu') = \exp\left[-\ln 2 \left(\frac{\nu'}{\nu_{\mathrm{IH}}}\right)^2\right] \tag{3}$$

where $G(\nu')$ is the inhomogeneous broadening function, the symbol * represents the convolution of two functions, ν_{IH} denotes the inhomogeneous bandwidth, and ν_{S} is the frequency of the scattered light.

Similarly, the $S_n \leftarrow S_1$ absorption spectrum is simulated by the following formulas:

$$A(\nu_0) \propto G(\nu')^* \left[\sum_{v} (E_{\mathrm{ev}} - E_{\mathrm{gi}}) |\langle \mathrm{v}|\mathrm{i}\rangle|^2 L_{\mathrm{v}}(\nu_0)\right] \tag{4}$$

$$L_{\mathrm{v}}(\nu_0) = \frac{1}{(E_{\mathrm{ev}} - E_{\mathrm{gi}} - h\nu_0)^2 + \Gamma_{\mathrm{H}}{}^2} \tag{5}$$

This is based upon the Franck−Condon principle, and the electronic transition is assumed to be broadened by both the homogeneous [Lorentzian, $L_{\mathrm{v}}(\nu_0)$] and inhomogeneous [Gaussian, $G(\nu')$] mechanisms.

In the simulation, only the three strongly Raman active olefinic modes, ν_7, ν_{13}, and ν_{15}, are first taken into account. Later, we will also try four-mode calculations, which include another mode in the low-wavenumber region. For the sake of simplicity, it is assumed that the molecular vibrations under consideration are harmonic and the Duschinsky rotations as well as the frequency changes on going from the S_1 to S_n state are absent. Then, the Franck−Condon factor in eqs 1 and 4 can be given by the following form:

$$\langle v|i\rangle = \prod_m \int \Psi_{im}(\xi_m) \Psi_{vm}(\xi_m - \Delta_m)\, \mathrm{d}\xi_m \tag{6}$$

where Ψ_{im} represents the harmonic oscillator eigenfunction for the *m*th normal mode with the quantum number *i*, ξ_m is the

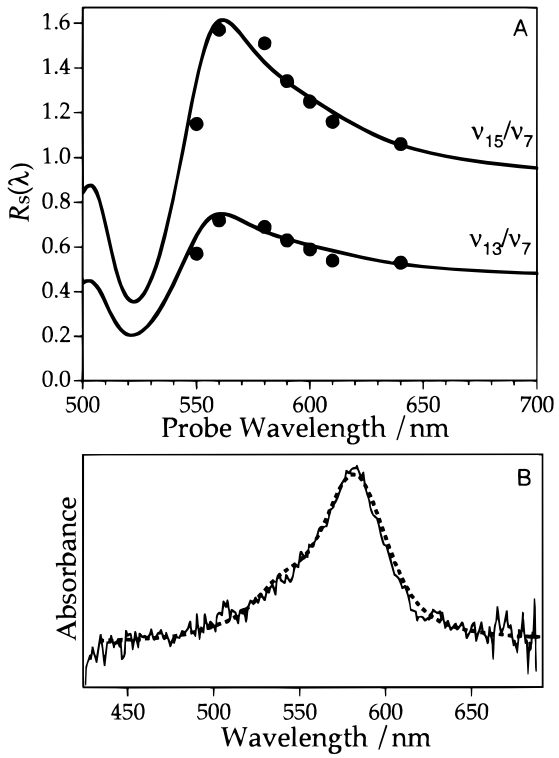

Figure 7. (A) Probe wavelength dependency of the Stokes Raman intensity ratio $R_s(\lambda)$: solid curves, simulated; filled circles, observed at 30 ps delay time. (B) Transient absorption spectrum of *trans*-stilbene in the S_1 state: solid curve, observed (from ref 41, pump wavelength is 306 nm and delay time is 58 ps); dotted curve, simulated.

dimensionless coordinate for the *m*th normal mode, and Δ_m's are the dimensionless displacements between the equilibrium positions of the S_1 and S_n states along the normal coordinates. The parameters Δ_i's, Γ_H, ν_{IH}, and E_0 (0−0 energy separation for the $S_n \leftarrow S_1$ transition) are adjusted to obtain good fits between the observed and simulated probe wavelength dependencies of the Stokes Raman intensities.

Molecules giving rise to the Stokes Raman scattering at 30 ps delay time in Figure 5 are mostly on the $n = 0$ level for high-wavenumber modes (i.e., the observed transition corresponds to $1 \leftarrow 0$). Thus, we simulate the Stokes REPs and the $S_n \leftarrow S_1$ absorption spectrum, assuming $n = 0$ for the vibrational modes under consideration. As mentioned in subsection 3.3, solvent Raman bands are not adequate as the intensity reference for determining the REPs of the photoexcited transient. Hence, the fitting procedure is performed on the relative Raman intensity of two bands, both of which are due to the S_1 species. Figure 7A shows the simulated and experimental probe wavelength dependency of the Stokes Raman intensity ratio. The ordinate indicates the ν_{15} or ν_{13} band intensity divided by the ν_7 band intensity [$R_s(\lambda) \equiv I_{15}(\lambda)/I_7(\lambda)$ or $I_{13}(\lambda)/I_7(\lambda)$, where $I_i(\lambda)$ denotes the Raman intensity of ν_i at Raman excitation (probe) wavelength λ]. All the observed points have been corrected for the ν_S^3 factor in eq 2. The parameters used for the simulation are $\Delta_7 = 0.42$, $\Delta_{13} = 0.35$, $\Delta_{15} = 0.52$, $\Gamma_H = 380\ cm^{-1}$, $\nu_{IH} = 420\ cm^{-1}$, and $E_0 = 17\,185\ cm^{-1}$. The agreement between the observed and simulated curves is satisfactory. Figure 7B shows the $S_n \leftarrow S_1$ absorption spectrum simulated with the same parameter set. The transient $S_n \leftarrow S_1$ absorption spectrum reported by Hochstrasser et al.[41] is also shown in this figure. The observed spectrum is satisfactorily reproduced by the simulation. These results for the Stokes REPs and the transient absorption give a solid basis to the analysis of anti-Stokes REPs to be discussed in the following subsection.

The bands assigned to the phenyl vibrations, ν_8 and ν_{16}, show probe wavelength dependencies different from those of the strong olefinic bands. In Figure 5, the intensity of the ν_{16} band is ~1/2 of that of the ν_{15} band in the 550 nm probe spectrum, while the ν_{16} band intensity is very weak in the 610 nm probe spectrum. The olefinic bands (ν_7, ν_{13}, and ν_{15}) show clear intensity maxima around the absorption maximum (~580 nm), whereas the intensity maximum is not clear for the ν_{16} band. Instead, the ν_{16} band intensity seems to increase almost monotonically as the probe wavelength becomes shorter. The ν_8 band shows a similar probe-wavelength dependency. Such characteristics cannot be explained by the model presently adopted, where only one resonant electronic transition ($S_n \leftarrow S_1$) is considered. A possible interpretation is that other electronic transitions located in the shorter wavelength (probably in the ultraviolet) region make significant contributions to the intensities of the phenyl ring bands. To discuss this point more quantitatively, measurements of the probe wavelength dependency of the Stokes and anti-Stokes Raman spectra in a much wider wavelength range are essential.

4.3. Probe Wavelength Dependency of Anti-Stokes Raman Spectra. An analysis of the anti-Stokes REPs is performed on the relative Raman intensity of two bands (ν_7 and ν_{15}) attributed to the S_1 transient, for the same reason as that mentioned in subsection 4.2 for the Stokes REPs. The anti-Stokes intensity depends on the population in the initial (vibrationally excited) state. Since the initial population is not known a priori, an independent intensity scale must be used for the simulation of each Raman band intensity in order to compare the experimental and simulated values. The ratio of the observed anti-Stokes intensity of the ν_{15} band to that of the ν_7 band at λ, $R_{as}(\lambda)$, is given by

$$R_{as}(\lambda) \equiv \frac{I_{15}(\lambda)}{I_7(\lambda)} = \frac{P_{15} I_{15}'(\lambda)}{P_7 I_7'(\lambda)} \tag{7}$$

where $I_7'(\lambda)$ and $I_{15}'(\lambda)$ are the calculated anti-Stokes Raman intensities and P_7 and P_{15} represent the populations on the initial vibrationally excited levels. The observed $I_{15}(\lambda)/I_7(\lambda)$ value cannot be compared with the calculated $I_{15}'(\lambda)/I_7'(\lambda)$, unless the P_{15}/P_7 value is available. However, it is possible to remove the P_{15}/P_7 factor by taking the following quantity, $r(\lambda)$, which may be called the anti-Stokes Raman relative intensity ratio.

$$r(\lambda) \equiv \frac{R_{as}(\lambda)}{R_{as}(\lambda_0)} = \frac{I_{15}(\lambda) I_7(\lambda_0)}{I_7(\lambda) I_{15}(\lambda_0)} = \frac{I_{15}'(\lambda) I_7'(\lambda_0)}{I_7'(\lambda) I_{15}'(\lambda_0)} \tag{8}$$

where λ_0 is an arbitrary wavelength chosen for a reference. Then, a direct comparison between the calculated and observed $r(\lambda)$ values is possible.

In Figure 8, $r(\lambda)$'s with $\lambda_0 = 660$ nm simulated for several initial levels are shown. In the cases treated in this figure, the energies of the initial levels are below the energy of the pump photon, i.e., 5200 cm^{-1} above the 0−0 band of the $S_1 \leftarrow S_0$ transition. The parameters used for the simulation are the same as those for Figure 7. The observed $r(\lambda)$ at 0 ps delay time is also shown in this figure (filled circles). Dependency of the detection sensitivity on the wavelength is found to be negligible in this wavelength region. The linearity of the Raman intensities against the pump power (see subsection 3.1) indicates that the effects of reabsorption of the scattered light by the transient species are also negligible. In the present study, we assume that the ν_7 and ν_{15} anti-Stokes Raman bands arise from a common excited level [(1,1), (1,2), (1,3), or (2,1), where n_7 and

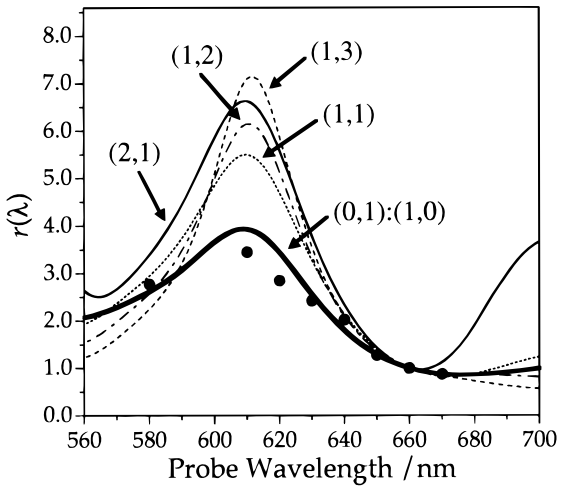

Figure 8. Probe wavelength dependency of the anti-Stokes Raman relative intensity ratio $r(\lambda)$ for $\lambda_0 = 660$ nm: filled circles, observed points at 0 ps delay time; curves, calculated by using the three-mode model with initial states (n_7, n_{15}), where n_7 and n_{15} of (n_7, n_{15}) represent the initial vibrational quantum numbers of the ν_7 and ν_{15} modes, respectively; (0,1):(1,0), calculated for the ν_{15} and ν_7 bands due to the (0,1) → (0,0) and (1,0) → (0,0) transitions, respectively.

n_{15} of (n_7, n_{15}) represent the initial vibrational quantum numbers of the ν_7 and ν_{15} modes, respectively] or from the lowest excited levels [(1,0) for the ν_7 band and (0,1) for the ν_{15} band]. If the vibrational excitation is extremely localized in the ν_7 mode, for example, this assumption is not correct. In this case, such a contribution that the ν_7 band arises from the initial state (2,0) while the ν_{15} band from (2,1) should also be considered. As shown in subsection 4.1, however, the pump wavelength dependency of the picosecond time-resolved anti-Stokes Raman spectra indicates that both the ν_7 and ν_{15} modes are substantially excited at 0 ps delay time, when the pump photons with a sufficiently high excess energy are used. The assumption mentioned above would therefore be valid.

Every simulated curve in Figure 8 shows a maximum at ~610 nm in agreement with the experimental observation. However, each curve has a different shape (wavelength dependency) and a different maximum $r(\lambda)$ value. Such features can be utilized for the determination of the initial state involved. The observed points are reproduced most properly in the (0,1):(1,0) curve, which is calculated on the assumption that both the ν_7 and ν_{15} bands arise from the lowest excited vibrational levels. This result suggests that the vibrationally excited transients at 0 ps delay time are mostly on the lowest excited vibrational levels of the S_1 state, as far as the ν_7 and ν_{15} modes are concerned.

trans-Stilbene in the S_1 state gives another strong low-wavenumber Raman band at 285 cm^{-1}, which is assigned to the C_o-C-C bend (ν_{24}, C_o represents the ethylenic carbon).[43] It was difficult to obtain reliable probe wavelength dependency data for this band with our present spectrograph because of interference by emission from the dye amplifier. To obtain information on the Franck−Condon factors relating to the ν_{24} mode, we need the Stokes intensity data for this band, at least for one probe wavelength. Then we tried to measure the Raman spectrum in the low-wavenumber region by the use of a narrow band-pass filter for the probe laser beam to reject the emission from the dye amplifier.

The Stokes Raman spectrum in the low-wavenumber region has been obtained with a satisfactory signal-to-noise ratio with a probe wavelength of 590 nm, which is shown in Figure 9. The intensity of the ν_{24} band is close to that of the ν_{15} band in Figure 9, in good agreement with the previous study.[43] We

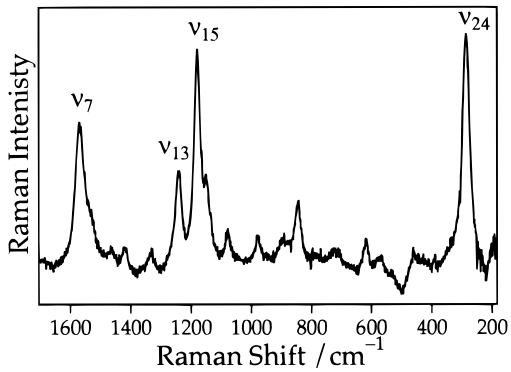

Figure 9. Stokes Raman spectrum of *trans*-stilbene in the S_1 state in the region 1700−200 cm^{-1} at 40 ps delay time. The Raman bands of 1-butanol (solvent) are subtracted. Pump, 295 nm; probe, 590 nm.

can now estimate the Δ_{24} value to reproduce the observed band intensities in Figure 9 and then to examine semiquantitatively the effects of the ν_{24} mode on the REPs of the other three modes. Calculation of the Raman intensities and the absorption spectrum has been performed on a four-mode model including the ν_7, ν_{13}, ν_{15}, and ν_{24} modes. The observed intensity of the ν_{24} band relative to that of the ν_{15} band is reproduced when the Δ_{24} value is set equal to 0.8−0.9. Since this Δ_{24} value is quite large, the other parameters for the simulation need to be changed slightly. The best fits between the calculated and observed results are obtained for the Stokes intensity profiles at 30 ps (Figure 7A), the electronic absorption (Figure 7B), and the ν_{24} band intensity at 590 nm (Figure 9), with the following parameter set: $\Delta_7 = 0.42$, $\Delta_{13} = 0.35$, $\Delta_{15} = 0.52$, $\Delta_{24} = 0.85$, $E_0 = 17\,085$ cm^{-1}, $\Gamma_H = 340$ cm^{-1}, and $\nu_{IH} = 380$ cm^{-1}. The excited vibrational levels of the ν_{24} mode may be significantly populated at room temperature. In the simulation, contributions from such thermally populated vibrationally excited states have been taken into consideration by assuming the Boltzmann distribution at room temperature.

With the parameters obtained, the anti-Stokes relative intensity ratios, $r(\lambda)$'s, are calculated, and the results are shown in Figure 10 together with the observed points at 0 ps. The curves in Figure 10A are calculated for the initial vibrational levels with $n_{24} = 0$ (i.e., the initial and final vibrational states for the Raman transitions involve the ground state for the ν_{24} mode), while those in Figure 10B are calculated for $n_{24} = 1$. The calculated curves for $n_{24} = 0$ (Figure 10A) are essentially the same as those in Figure 8. In contrast, in the calculated curves for $n_{24} = 1$ (Figure 10B), the maximum values of $r(\lambda)$ are seriously smaller than those in Figures 8 and 10A. This result suggests that if the vibrationally excited populations on the $n_{24} \geq 1$ levels are significantly large, the curves calculated for the initial vibrational levels other than the lowest ones [the (1,1) curve, for example] may be the best fit to the observed points.

However, it is unlikely that the $n_{24} \geq 1$ populations in the S_1 state are very large under the present condition as discussed in the following. To populate the $n_{24} \geq 1$ levels, the ν_{24} mode should be highly excited on the $S_1 \leftarrow S_0$ photoexcitation. In other words, the displacement between the equilibrium geometries of the S_0 and S_1 states along this mode should be large. However, the displacement along the ν_{24} mode is considered to be small because no strong band attributable to the ν_{24} mode is observed in the Raman spectrum of *trans*-stilbene (in the S_0 state) in resonance with the $S_1 \leftarrow S_0$ transition.[40] This means that the ν_{24} mode is not highly excited on the $S_1 \leftarrow S_0$ photoexcitation and that the populations on $n_{24} \geq 1$ in the S_1 state are primarily due to the distribution at a thermal equilib-

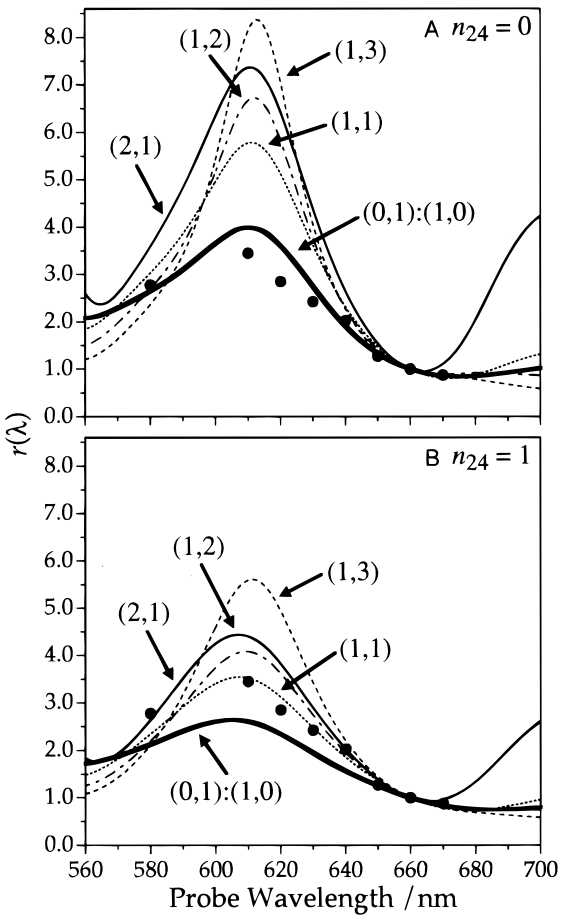

Figure 10. Probe wavelength dependency of the anti-Stokes Raman relative intensity ratio $r(\lambda)$ for $\lambda_0 = 660$ nm: filled circles, observed points at 0 ps delay time; curves, calculated by using the four-mode model including the ν_{24} mode with the initial states (n_7, n_{15}) (see caption for Figure 8). The vibrational quantum number of the ν_{24} mode (n_{24}) is shown on the each panel.

rium. In a thermal equilibrium, the ratio of the population of the $n_{24} = 1$ level to that of the $n_{24} = 0$ level is estimated to be ~0.25 at room temperature and ~0.47 at 550 K (calculated maximum temperature for the excess energy distributed statistically among all the intramolecular vibrational modes). Therefore, it can be considered that the populations on the $n_{24} \geq 1$ levels are not large in the present case; in other words, about 70−80% of the molecules in the S_1 state at 0 ps delay time exist on the $n_{24} = 0$ level.

Although the major contribution to the anti-Stokes Raman intensity may be from the $n_{24} = 0$ levels, it should still be noted that the populations on the $n_{24} \geq 1$ levels are not negligible even at room temperature. If we take the weighted average of the $r(\lambda)$'s for various n_{24} values, using the weights calculated on the Boltzmann distribution at room temperature, the (0,1):(1,0) curve gives the best fit to the experimental points. If the vibrational temperature for the ν_{24} mode exceeds 550 K, on the other hand, the weighted average of the $r(\lambda)$'s based on the (1,1) curve becomes the best fit. The vibrational temperature for ν_{24} is not clear at present, but it is hard to consider that the temperature exceeds 550 K. Consequently, the observed initial state is most probably the lowest excited vibrational states for the ν_7 and ν_{15} modes. The curves for (1,2), (1,3), and (2,1) do not fit the experimental data within the realistic temperature range. Thus, it is highly unlikely that the vibrational quantum numbers for the ν_7 and ν_{15} modes are two or higher for the observed vibrationally excited transients. From the weak Raman

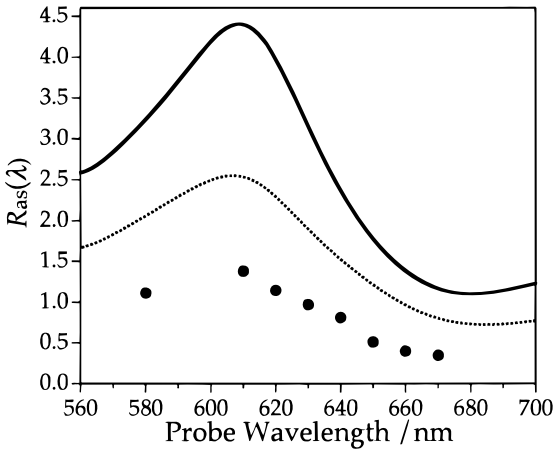

Figure 11. Probe wavelength dependency of the anti-Stokes Raman intensity ratio $R_{as}(\lambda)$: solid curve, calculated for a thermal equilibrium at 550 K; dotted curve, calculated for a thermal equilibrium at 1000 K; filled circles, observed points at 0 ps delay time.

intensities, the Δ values for vibrational modes other than ν_7, ν_{13}, ν_{15}, and ν_{24} are considered to be small, and these vibrational modes may have only minor effects on $r(\lambda)$.

To summarize, the probe wavelength dependency of the anti-Stokes Raman spectrum suggests that the vibrationally excited transients observed in the SWP spectrum at 0 ps delay time are mostly on the lowest excited vibrational levels of the ν_7 and ν_{15} modes. This result suggests that highly excited vibrational levels of the ν_7 and ν_{15} modes, which are generated immediately after the photoexcitation, relax very rapidly (probably in the femto to subpicosecond time range) to the lowest excited vibrational levels of these modes.

As discussed in subsection 4.1, it has been concluded from the pump wavelength dependency of the anti-Stokes Raman spectra that the SWP spectrum at 0 ps delay time arises from vibrationally excited transients with the excess vibrational energy not thermally distributed in the molecule. This point is discussed here again in terms of the probe wavelength dependency of the anti-Stokes spectra. To examine this point, we calculate the $R_{as}(\lambda)$ assuming that the excess energy is thermally distributed and compare the result with the observed value at 0 ps delay time. In a thermal equilibrium, the P_{15}/P_7 factor in eq 7 corresponds to the ratio of the Boltzmann factors for the $n = 1$ levels of the ν_{15} and ν_7 modes. The simulated $R_{as}(\lambda)$ at 550 K is shown in Figure 11, together with the observed $R_{as}(\lambda)$ at 0 ps delay time. The ν_{24} mode is included in this simulation ($\Delta_{24} = 0.85$). In Figure 11, the simulated $R_{as}(\lambda)$ values are substantially larger than the observed points. The calculated $R_{as}(\lambda)$ at a temperature of 1000 K is also shown in this figure. The discrepancy between the calculated and observed results is still large. Hence, to explain the experimental results on the basis of the Boltzmann distribution, the temperature of the excited species must be assumed to be much higher than 1000 K, which is clearly unrealistic. Therefore, it is concluded that the anti-Stokes scattering obtained at 0 ps delay time arises from molecules in which the excess energy (part of the initial excess energy) is more localized in the ν_7 mode than in the ν_{15} mode.

4.4. Vibrational Relaxation Dynamics of *trans*-Stilbene in the S_1 State. From the present study based on the analysis of the pump and probe wavelength dependencies of the anti-Stokes Raman spectra, it is suggested that the intramolecular vibrational relaxation process of *trans*-stilbene in the S_1 state proceeds in roughly two steps. In the molecule in the S_1 state immediately after SWP photoexcitation, the olefinic stretching

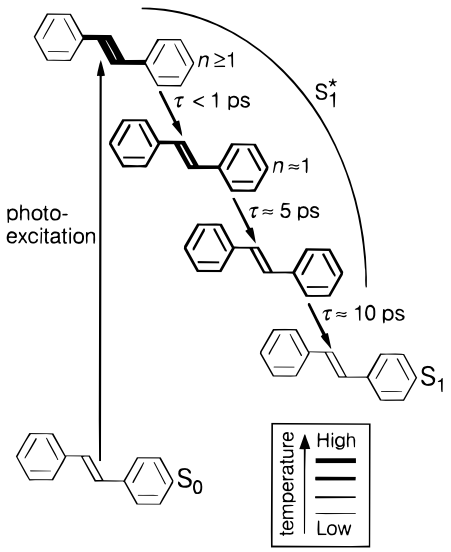

Figure 12. Schematic diagram of the vibrational relaxation process of *trans*-stilbene in the S_1 state in solution. Moieties drawn with thick lines represent the vibrationally hot part, while those with fine lines depict the cold part.

(ν_7 and ν_{15}) modes are highly excited, and the molecule relaxes very rapidly (in the femto to subpicosecond time range) to the lowest excited vibrational levels of these modes. In this stage, part of the excess energy remains localized in the ν_7 and ν_{15} modes. Then, slower relaxation (in several picoseconds) occurs to give an intramolecular (quasi) thermal equilibrium. This means that, even in a large molecule such as *trans*-stilbene, there is a bottleneck state in the intramolecular vibrational relaxation process in solution.[6] A schematic diagram representing the vibrational relaxation process mentioned above is shown in Figure 12.

The above conclusion suggests that, in the relaxation process of vibrationally highly excited states after SWP photoexcitation, a large part (3000−4000 cm^{-1}) of the excess energy is transferred from the Franck−Condon active high-wavenumber modes to energy acceptors in the time range of femto- to subpicoseconds. Two possible energy acceptors are conceivable: (a) other intramolecular vibrational modes including Raman-inactive dark modes and low-wavenumber modes and (b) surrounding solvent molecules.

In the case of (a), it is likely that the excess energy is distributed among only a limited number of vibrational modes at the fast relaxation stage (this situation is similar to the "intermediate case" of relatively small molecules[44]), since the present study has shown that a nonstatistical distribution persists for several picoseconds after photoexcitation. In the case of (b), a very rapid transfer of the excess energy to solvent molecules should be assumed. This assumption may seem to be inconsistent with the generally accepted view[35,41] that it takes at least tens of picoseconds for vibrationally excited molecules to reach a thermal equilibrium with surrounding solvent molecules. However, it is conceivable that the energy-transfer rate strongly depends on the excess energy; the rate greatly increases if the excess energy is high.

In the present study, we cannot determine which of the two pathways dominates in the ultrafast vibrational relaxation of *trans*-stilbene in the S_1 state. More elaborate measurements (such as measurements with higher temporal resolution, pump and probe in wider wavelength regions, excitation with a much more stable light source, etc.) and analyses are needed to reach a more definitive conclusion on this point.

References and Notes

(1) Laubereau, A.; Kaiser, W. *Rev. Mod. Phys.* **1978**, *50*, 607.
(2) Oxtoby, D. W. *Annu. Rev. Phys. Chem.* **1981**, *32*, 77.
(3) Oxtoby, D. W. *Adv. Chem. Phys.* **1981**, *47*, 487.
(4) Heilweil, E. J.; Casassa, M. P.; Cavanagh, R. R.; Stephenson, J. C. *Annu. Rev. Phys. Chem.* **1989**, *40*, 143.
(5) Elsaesser, T.; Kaiser, W. *Annu. Rev. Phys. Chem.* **1991**, *42*, 83.
(6) Owrutsky, J. C.; Raftery, D.; Hochstrasser, R. M. *Annu. Rev. Phys. Chem.* **1994**, *45*, 519.
(7) Tokmakoff, A.; Zimdars, D.; Urdahl, R. S.; Francis, R. S.; Kwok, A. S.; Fayer, M. D. *J. Phys. Chem.* **1995**, *99*, 13310.
(8) In the area of the gas-phase spectroscopy, the term "IVR" sometimes has a slightly different meaning. In the present paper, following the generally accepted definition in the area of the liquid-phase spectroscopy,[16−19] we use this term for the process that is completed with randomization of the excess energy.
(9) Sension, R. J.; Szarka, A. Z.; Hochstrasser, R. M. *J. Chem. Phys.* **1992**, *97*, 5239.
(10) Todd, D. C.; Fleming, G. R.; Jean, J. M. *J. Chem. Phys.* **1992**, *97*, 8915.
(11) Sension, R. J.; Repinec, S. T.; Szarka, A. Z.; Hochstrasser, R. M. *J. Chem. Phys.* **1993**, *98*, 6291.
(12) Lenz, K.; Pfeiffer, M.; Lau, A.; Elsaesser, T. *Chem. Phys. Lett.* **1994**, *229*, 340.
(13) Chudoba, C.; Lutgen, S.; Jentzsch, T.; Riedle, E.; Woerner, M.; Elsaesser, T. *Chem. Phys. Lett.* **1995**, *240*, 35.
(14) Doig, S. J.; Reid, P. J.; Mathies, R. A. *J. Phys. Chem.* **1991**, *95*, 6372.
(15) Schneebeck, M. C.; Vigil, L. E.; Ondrias, M. R. *Chem. Phys. Lett.* **1993**, *215*, 251.
(16) Sato, S.; Kitagawa, T. *Appl. Phys. B* **1994**, *59*, 415.
(17) Shreve, A. P.; Mathies, R. A. *J. Phys. Chem.* **1995**, *99*, 7285.
(18) Qian, J.; Schultz, S. L.; Jean, J. M. *Chem. Phys. Lett.* **1995**, *233*, 9.
(19) Schultz, S. L.; Qian, J.; Jean, J. M. *J. Phys. Chem. A* **1997**, *101*, 1000.
(20) Matousek, P.; Parker, A. W.; Toner, W. T.; Towrie, M.; de Faria, D. L. A.; Hester, R. E.; Moore, J. N. *Chem. Phys. Lett.* **1995**, *237*, 373.
(21) Kruglik, S. G.; Mizutani, Y.; Kitagawa, T. *Chem. Phys. Lett.* **1997**, *266*, 283.
(22) Mizutani, Y.; Kitagawa, T. *Science* **1997**, *278*, 443.
(23) Nakabayashi, T.; Okamoto, H.; Tasumi, M. *J. Phys. Chem. A* **1997**, *101*, 7189.
(24) Xu, X.; Lingle, R., Jr.; Yu, S. C.; Chang, Y. J.; Hopkins, J. B. *J. Chem. Phys.* **1990**, *92*, 2106.
(25) Lingle, R., Jr.; Xu, X.; Zhu, H.; Yu, S. C.; Hopkins, J. B. *J. Am. Chem. Soc.* **1991**, *113*, 3992.
(26) Lingle, R., Jr.; Xu, X.; Zhu, H.; Yu, S. C.; Hopkins, J. B. *J. Phys. Chem.* **1991**, *95*, 9320.
(27) Brack, T. L.; Atkinson, G. H. *J. Phys. Chem.* **1991**, *95*, 2351.
(28) Hayashi, H.; Brack, T. L.; Noguchi, T.; Tasumi, M.; Atkinson, G. H. *J. Phys. Chem.* **1991**, *95*, 6797.
(29) Phillips, D. L.; Rodier, J.-M.; Myers, A. B. *Chem. Phys.* **1993**, *175*, 1.
(30) Nakabayashi, T.; Okamoto, H.; Tasumi, M. *J. Raman Spectrosc.* **1995**, *26*, 841.
(31) Huang, Y.; Hopkins, J. B. *J. Phys. Chem.* **1996**, *100*, 9585.
(32) Okamoto, H.; Nakabayashi, T.; Tasumi, M. *J. Phys. Chem. A* **1997**, *101*, 3488.
(33) Nakabayashi, T.; Okamoto, H.; Tasumi, M. *J. Phys. Chem. A* **1997**, *101*, 3494.
(34) Hamaguchi, H. In *Vibrational Spectra and Structure*; Durig, J. R., Ed.; Elsevier: Amsterdam, 1987; Vol. 16, pp 227−309.
(35) Hamaguchi, H.; Gustafson, T. L. *Annu. Rev. Phys. Chem.* **1994**, *45*, 593.
(36) Okamoto, H.; Tasumi, M. *Rev. Sci. Instrum.* **1995**, *66*, 5165.
(37) Urano, T.; Hamaguchi, H.; Tasumi, M.; Yamanouchi, K.; Tsuchiya, S.; Gustafson, T. L. *J. Chem. Phys.* **1989**, *91*, 3884.
(38) Iwata, K.; Hamaguchi, H. *J. Raman Spectrosc.* **1994**, *25*, 615.
(39) Dyck, R. H.; McClure, D. S. *J. Chem. Phys.* **1962**, *36*, 2326.
(40) Myers, A. B.; Trulson, M. O.; Mathies, R. A. *J. Chem. Phys.* **1985**, *83*, 5000.
(41) Hochstrasser, R. M. *Pure Appl. Chem.* **1981**, *52*, 2683.
(42) Iwata, K.; Weaver, W. L.; Gustafson, T. L. *Chem. Phys. Lett.* **1993**, *210*, 50.
(43) Hamaguchi, H. *J. Mol. Struct.* **1985**, *126*, 125.
(44) Medvedev, E. S.; Oscherov, V. I. *Radiationless Transitions in Polyatomic Molecules*; Springer: Berlin, 1995.